INSTITUTE OF PHYSICS PUBLISHING MEASUREMENT SCIENCE AND TECHNOLOGY

Meas. Sci. Technol. **18** (2007) 755–763 doi:10.1088/0957-0233/18/3/027

Variational estimation of experimental fluid flows with physics-based spatio-temporal regularization

Paul Ruhnau, Annette Stahl and Christoph Schnörr

Computer Vision, Graphics, and Pattern Recognition Group, Department of Mathematics and Computer Science, University of Mannheim, D-68131 Mannheim, Germany

E-mail: ruhnau@uni-mannheim.de, astahl@uni-mannheim.de and schnoerr@uni-mannheim.de

Received 21 August 2006, in final form 28 November 2006
Published 24 January 2007
Online at stacks.iop.org/MST/18/755

Abstract
We present a variational approach to motion estimation of instationary experimental fluid flows from image sequences. Our approach extends prior work along two directions: (i) the full incompressible Navier–Stokes equation is employed in order to obtain a physically consistent regularization which does not suppress turbulent variations of flow estimates; (ii) regularization along the time axis is employed as well, but formulated in a receding horizon manner in contrast to previous approaches to spatio-temporal regularization. This allows for a recursive on-line (non-batch) implementation of our variational estimation framework. Ground-truth evaluations for simulated turbulent flows demonstrate that due to imposing both physical consistency and temporal coherency, the accuracy of flow estimation compares favourably even with advanced cross-correlation approaches and optical flow approaches based on higher order div–curl regularization.

Keywords: particle image velocimetry, optical flow, Navier–Stokes equation, variational methods, mixed finite elements

(Some figures in this article are in colour only in the electronic version)

1. Introduction

1.1. Overview and motivation

Image sequence analysis of fluid flows constitutes an active research field with a high industrial impact. Corresponding real-world measurements in concrete scenarios complement numerical results from direct simulations of the Navier–Stokes equation, particularly in the case of turbulent flows, and for the understanding of the complex spatio-temporal evolution of instationary flow phenomena. More and more advanced imaging devices (lasers, high-speed cameras, control logic, etc) are currently developed that allow us to record fully time-resolved image sequences of fluid flows at high resolutions. As a consequence, there is a need for advanced algorithms for the analysis of such data, to provide the basis for a subsequent pattern analysis, and with abundant applications across various areas.

The image measurement process proceeds as follows: first, the flow medium is seeded with small particles that are designed such that they accurately follow the fluid's motion. Next, entire velocity fields are measured by taking two or more images of the flow within short time intervals, and by estimating and interpolating the displacements of individual particles from frame to frame.

A basic requirement for any motion estimation scheme in this connection is physical consistency. Otherwise, the information provided by a subsequent motion analysis is limited. Current approaches to PIV [19] do not address this issue *as part of* the motion estimation scheme. As a consequence, this calls for a novel combination of motion

estimation and the Navier–Stokes equation which governs the real unknown flow in all applications.

Our contribution reported in this paper is a novel spatio-temporal variational approach to the estimation of motion fields constrained by the Navier–Stokes equation.

1.2. Related work

Recently, variational optical flow techniques from the field of computer vision have been adopted and extended for the purpose of PIV [5, 10, 20–22]. Besides combining a carefully designed data term and coarse-to-fine estimation schemes with a standard first-order regularizer [21], a physically more plausible regularization has been suggested recently [22]. Because this approach is based on the Stokes equation, however, it is based on related assumptions which are strictly valid only for low Reynold numbers, i.e. *non-turbulent* flow. Another competitive research direction concerns the design and use of higher order regularizers [5, 10, 27]. By separately penalizing the *gradient* of the divergence and the curl of flows, the major disadvantage of first-order regularization that penalizes flow variations too much is alleviated. Issues such as well posedness, accurated discretization and numerical stability, on the other hand, become more involved.

To add physically motivated prior knowledge to cross-correlation PIV methods, physics-based nonlinear dynamic models [16] have been introduced. The velocity is obtained by minimizing a measure which consists of the residues of the Navier–Stokes equation, the continuity equation, and the difference between estimated and observed image data. The resulting nonlinear optimization system is solved using methods from evolutionary programming [13]. This procedure is repeated until the difference between the observed and the estimated image is sufficiently small. This method allows a reliable estimation of velocity fields and pressure estimates.

One may criticize, however, that little insight can be gained from the viewpoint of optimization because a general-purpose framework for intricate problems was used (evolutionary programming). It does not take into account the structure of the underlying problem. This is in contrast to our approach presented below where the computational flow estimation scheme with provable properties (well posedness, numerical stability) is directly derived from an adequate variational problem formulation.

Finally, we point out that the vorticity transport equation has been used before in the field of computer vision in order to 'inpaint' images and videos (cf, e.g., [1] and [17, chapter 3]). In this completely different context, the same transport mechanism is used to infer from surrounding image parts *spatial* image structures within local image regions that may result from removing corrupted image parts, disturbing text, etc.

1.3. Contribution

We present a framework for fluid motion estimation that utilizes as prior knowledge the fact that flows have to satisfy the incompressible vorticity transport equation. This equation relates to the full (incompressible) Navier–Stokes equations and therefore is also valid in *turbulent* scenarios. Furthermore, rather than considering image pairs, our estimation scheme takes into account the whole image sequence. As a result, it takes into account previous estimation results so as to enforce spatio-temporal coherency and regularization, however, *without* penalizing flow structures that are characteristic of instationary turbulent flows. Finally, analogous to the corresponding concept from control theory, our overall algorithm works in a receding horizon manner, that is flow velocities can be computed as soon as their respective frames have been recorded. By this, we avoid a significant part of the computational costs associated with common temporal regularization and control schemes [7, 26].

1.4. Organization

We sketch in section 2.1 the derivation of the vorticity transport equation, which embodies the prior knowledge we use for flow estimation. Section 2.2 motivates and describes our variational approach and details the resulting constrained optimization problem. Corresponding numerical issues are dealt with in section 3. Numerical experiments for evaluating the approach are presented in section 4. We conclude and indicate further research directions in section 5.

2. Approach

2.1. The vorticity transport equation

Let $u = (u_1, u_2)^\top, u = u(x,t), x = (x_1(t), x_2(t))^\top$ denote a two-dimensional velocity field. The Navier–Stokes equation, the governing equation for incompressible homogeneous flow (density $\rho = \rho_0 = \text{const}$), reads

$$\frac{\partial u}{\partial t} + (u \cdot \nabla)u = -\nabla p' + \nu \Delta u, \qquad \nabla \cdot u = 0, \tag{1}$$

where ν is the coefficient of kinematic viscosity and $p' = p/\rho_0$. Applying $\nabla\times$ to the Navier–Stokes equation[1], we obtain

$$\nabla \times \frac{\partial u}{\partial t} + \nabla \times (u \cdot \nabla)u = -\nabla \times \nabla p' + \nu \nabla \times \Delta u. \tag{2}$$

Taking into account the incompressibility constraint $\nabla \cdot u = 0$, and by setting $\omega = \nabla \times u$, it follows from elementary calculus that (2) can be rewritten as

$$\frac{\mathrm{D}\omega}{\mathrm{D}t} = \frac{\partial}{\partial t}\omega + u \cdot \nabla\omega = \nu \Delta\omega, \qquad \omega(x,0) = \omega_0. \tag{3}$$

This equation is known as the *vorticity transport equation*. It describes the evolution of the fluid's vorticity over time. Note that in the absence of external forces acting on the fluid, this equation describes the flow completely.

2.2. Variational model

Let $I(x_1, x_2, t)$ denote the grey value of an image sequence recorded at location $x = (x_1, x_2)^\top$ within some rectangular image domain Ω and time $t \in [0, T]$. We adopt the basic assumption underlying most approaches to motion estimation that I is conserved. Thus, the total (material) derivative of I vanishes:

$$\frac{\mathrm{D}I}{\mathrm{D}t} = u \cdot \nabla I + I_t = 0. \tag{4}$$

[1] Throughout this paper, we consider 2D flows only. We therefore define $\nabla \times u = \frac{\partial u_2}{\partial x_1} - \frac{\partial u_1}{\partial x_2}$.

The spatial and temporal derivatives of I of the optical flow constraint (4) are estimated locally by using FIR filters. As the focus of this paper is on physically consistent regularization and not on design of the data term, we refer the interested reader to [21] for a detailed description.

As is well known, equation (4) alone cannot be used to reconstruct the velocity field u, because *any* vector field with components $u \cdot \nabla I = -I_t$ at each location x satisfies (4).

The standard approach is to minimize the squared residual of (4) over the entire image domain Ω and to add a variational term that either enforces smoothness of the flow (*first-order* regularization) [24][2]

$$\int_\Omega \{(u \cdot \nabla I + I_t)^2 + \alpha |\nabla \cdot u|^2 + \beta |\nabla \times u|^2\} \, \mathrm{d}x, \tag{5}$$

or smoothness of the divergence and vorticity (*second-order* regularization) [25]

$$\int_\Omega \{(u \cdot \nabla I + I_t)^2 + \alpha |\nabla(\nabla \cdot u)|^2 + \beta |\nabla(\nabla \times u)|^2\} \, \mathrm{d}x. \tag{6}$$

We emphasize that both approaches (5) and (6) take only into account *spatial* context and determine a vector field for a *fixed* point in time $t \in [0, T]$.

Therefore, following the ideas of [23], our present work is an attempt to elaborate a *dynamic* representation of fluid flow. To this end, we solve equation (3) for the time interval $[0, T]$ between a subsequent pair of image frames, where ω_0 denotes our current vorticity estimate. As a result, we obtain a *transported* vorticity field $\omega_T := \omega(x, T)$, which can be regarded as a *predicted* vorticity based on the assumption that our fluid is governed by the Navier–Stokes equation. The regularization term that we employ penalizes derivations from the predicted vorticity values and forces incompressibility:

$$\begin{aligned} &\frac{1}{2} \int_\Omega \{(u \cdot \nabla I + I_t)^2 + \lambda (\nabla \times u - \omega_T)^2\} \, \mathrm{d}x, \\ &\text{s.t.} \quad \nabla \cdot u = 0. \end{aligned} \tag{7}$$

We apply Neumann boundary conditions (i.e., $\partial u / \partial n = 0$ on $\partial\Omega$). Note that, while the regularization term of (7) penalizes deviations between the current vorticity estimate ω and the propagated vorticity estimate of the preceding frame ω_T, it does *not* enforce smoothness of the current vorticity. In practice, an implementation of (7) therefore leads to increasingly noisy vorticity estimates. Increasing the parameter ν reduces the problem only slightly: ω_T becomes smoother, but smoothness of ω is still not enforced directly.

To overcome this problem, we add a term that mimics the small viscous term (Laplacian) on the right-hand side of equation (3). Expressing the new second-order regularization term equivalently through a first-order regularizer and an additional linear constraint, we finally obtain

$$\begin{aligned} &E = \frac{1}{2} \int_\Omega \{(u \cdot \nabla I + I_t)^2 + \lambda (\omega - \omega_T)^2 + \kappa |\nabla \omega|^2\} \, \mathrm{d}x, \\ &\text{s.t.} \quad \nabla \cdot u = 0, \qquad \nabla \times u = \omega. \end{aligned} \tag{8}$$

As we usually do not have a vorticity estimate at the very first frame of an image sequence, the overall estimation process is initialized with a vorticity estimate $\omega_0 = 0$.

[2] It can be shown easily that the Horn and Schunck approach [9] is just the special case of this regularization where $\alpha = \beta$.

The novel vorticity transport regularizer in (8), in connection with (3), can be perceived as a *special second-order div–curl regularizer*: estimated flows from a given image sequence have vanishing divergence and a curl field (vorticity) that should be smooth and as close as possible to the transported vorticity.

3. Discretization and optimization

3.1. Discretization of the vorticity transport equation

We solve the time-dependent vorticity transport equation (3) with a second-order conservative finite difference scheme. The method is upwind and two-dimensional in that the numerical fluxes are obtained by solving the characteristic form at cell edges (i.e., edges between adjacent pixels), and all fluxes are evaluated and differenced at the same time. The finite difference method that we employ is the Fromm–Van-Leer scheme [18].

The basic idea is to satisfy Godunov's theorem in a 'natural' way. Roughly speaking, Godunov's theorem says that all methods of accuracy greater than order one will produce spurious oscillations in the vicinity of large gradients, while being second-order accurate in regions where the solution is smooth. Accordingly, Fromm–Van-Leer's scheme detects discontinuities and adapts its behaviour such that the higher-order accuracy of Fromm's scheme is preserved for smooth parts of the solution, while spurious oscillations are avoided through first-order accuracy at detected discontinuities. For further details, we refer to [18].

3.2. Variational approach

For every image pair (two consecutive frames of the image sequence), we have to solve the optimization problem (8) which comprises a convex functional and two linear constraint equations. We transform this constrained optimization problem into a saddle point problem. Accordingly, the unique vector field $u(x)$ minimizing (8), along with the vorticity ω and multipliers p, q, are determined by the variational system

$$\begin{aligned} &a((u, \omega)^\top, (\tilde{u}, \tilde{\omega})^\top) + b((p, q)^\top, (\tilde{u}, \tilde{\omega})^\top) \\ &\quad = ((f, g)^\top, (\tilde{u}, \tilde{\omega})^\top), \qquad \forall \tilde{u}, \tilde{\omega} \\ &b((\tilde{p}, \tilde{q})^\top, (u, \omega)^\top) = 0, \qquad \forall \tilde{p}, \tilde{q}. \end{aligned} \tag{9}$$

The bilinear and linear forms read

$$\begin{aligned} &a((u, \omega)^\top, (\tilde{u}, \tilde{\omega})^\top) \\ &\quad := \int_\Omega \{u \cdot \nabla I \nabla I \cdot \tilde{u} + \lambda \omega \tilde{\omega} + \kappa \nabla \omega \cdot \nabla \tilde{\omega}\} \, \mathrm{d}x, \\ &b((p, q)^\top, (\tilde{u}, \tilde{\omega})^\top) := - \int_\Omega \{p \nabla \cdot \tilde{u} + q(\nabla \times \tilde{u} - \tilde{\omega})\} \, \mathrm{d}x. \end{aligned} \tag{10}$$

The right-hand side reads

$$((f, g)^\top, (\tilde{u}, \tilde{\omega})^\top) := \int_\Omega \{-I_t \nabla I \cdot \tilde{u} + \lambda \omega_T \tilde{\omega}\} \, \mathrm{d}x. \tag{11}$$

We choose a regular tessellation of the image domain Ω and discretize (9) using finite elements. It is well known from computational fluid dynamics (cf Stokes equation) that standard first-order finite element discretizations of saddle

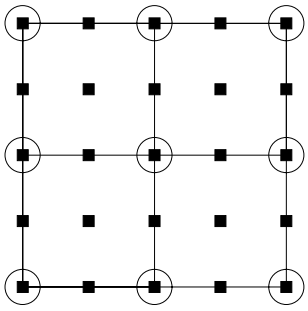

Figure 1. Sketch of 2D Taylor–Hood elements: biquadratic velocity elements (squares) and bilinear pressure elements (circles).

point problems may result in instabilities or even in so-called locking effects, where the zero velocity field is the only one satisfying the incompressibility condition. Therefore, when solving saddle point problems, mixed finite elements are traditionally used [3]. An admissible choice is the so-called Taylor–Hood element based on a square reference element with nine nodes (figure 1). Each component of the velocity field is defined in terms of piecewise quadratic basis functions ψ_i located at each node (the solid squares in figure 1), whereas the Lagrange multipliers p and q and the vorticity ω are represented by linear basis functions ϕ_i attached to each corner node (indicated by circles in figure 1). The graphs of these basis functions are depicted in figure 2. It can be shown that Taylor–Hood elements fulfil the so-called Babuska–Brezzi condition [3], making the discretized problem well posed.

Indexing the velocity nodes (squares in figure 1) by $1, 2, \ldots, N$, we obtain

$$u_1(x) = \sum_{i=1}^{N} u_i \psi_i(x) \tag{12}$$

and similarly for $u_2(x)$ (where $u = (u_1, u_2)^\top$) and the components of $\tilde{u}$. By analogy, we obtain for the M Lagrange multiplier nodes (circles in figure 1)

$$p(x) = \sum_{i=1}^{M} p_i \phi_i(x) \tag{13}$$

and similarly expressions for $q, \omega, \tilde{p}, \tilde{q}, \tilde{\omega}$. Hence, each function $u, \tilde{u}$ is represented by $2N$ real variables, and each function $p, q, \omega, \tilde{p}, \tilde{q}, \tilde{\omega}$ is represented by M real variables. For the sake of simplicity, we will use the same symbols to denote the corresponding vectors. The discretized system (10) then reads

$$\begin{aligned} &A(u,\omega)^\top \cdot (\tilde{u},\tilde{\omega})^\top + B^\top (p,q)^\top \cdot (\tilde{u},\tilde{\omega})^\top \\ &\quad = (f,g)^\top \cdot (\tilde{u},\tilde{\omega})^\top, \qquad \forall \tilde{u},\tilde{\omega} \\ &B(u,\omega)^\top \cdot (\tilde{p},\tilde{q})^\top = 0, \qquad \forall \tilde{p},\tilde{q}. \end{aligned} \tag{14}$$

Because these equations have to be satisfied for *arbitrary* $\tilde{u}, \tilde{p}, \tilde{q}, \tilde{\omega}$, we finally obtain

$$A \begin{pmatrix} u \\ \omega \end{pmatrix} + B^\top \begin{pmatrix} p \\ q \end{pmatrix} = \begin{pmatrix} f \\ g \end{pmatrix}, \qquad B \begin{pmatrix} u \\ \omega \end{pmatrix} = 0. \tag{15}$$

In order to numerically solve the saddle point problem (15), we want to employ the Uzawa algorithm (cf, e.g., [2]). However, this requires A to be positive definite which is not the case here, because the relations u and ω defining A in (10) are mutually independent and u is only involved through a degenerate quadratic form. This problem can be removed by

- including a penalty term related to the divergence constraint into our Lagrange multiplier formulation to obtain an augmented Lagrangian formulation [6], and by
- splitting the vorticity matching term into two equivalent terms, one containing $\nabla \times u$ and the other one containing ω.

This yields the following modification of the bilinear form (10):

$$\begin{aligned} &a_p((u,\omega)^\top, (\tilde{u},\tilde{\omega})^\top) \\ &:= \int_\Omega \Big\{ u \cdot \nabla I \nabla I \cdot \tilde{u} + \frac{\lambda}{2}(\omega\tilde{\omega} + (\nabla \times u)(\nabla \times \tilde{u})) \\ &\quad + \mu(\nabla \cdot u)(\nabla \cdot \tilde{u}) + \kappa \nabla\omega \cdot \nabla\tilde{\omega} \Big\} \mathrm{d}x. \end{aligned} \tag{16}$$

We point out that this modification is done for numerical reasons only. It does not change the optimization problem (8). Matrix A_p resulting from the discretization of (16) is positive definite and, because u and ω do *not explicitly* depend on each other, can be split into two systems:

- The system containing u is the linear system with a simple first-order div–curl regularization (cf, e.g., [24], and (5)).
- The system containing ω corresponds to a simple first-order quadratic functional.

Because A_p is invertible and well conditioned, we solve the first equation of the system (15), with A replaced by A_p, for the unknown u

$$\begin{pmatrix} u \\ \omega \end{pmatrix} = A_p^{-1} \left[\begin{pmatrix} f \\ g \end{pmatrix} - B^\top \begin{pmatrix} p \\ q \end{pmatrix} \right], \tag{17}$$

and insert the result into the second equation:

$$B A_p^{-1} \left[\begin{pmatrix} f \\ g \end{pmatrix} - B^\top \begin{pmatrix} p \\ q \end{pmatrix} \right] = 0. \tag{18}$$

This problem only involves the adjoint variables p, q:

$$\left(B A_p^{-1} B^\top\right) \begin{pmatrix} p \\ q \end{pmatrix} = B A_p^{-1} \begin{pmatrix} f \\ g \end{pmatrix}. \tag{19}$$

The matrix $\left(B A_p^{-1} B^\top\right)$ is symmetric and positive definite. Therefore, we apply the conjugate gradient iteration to (19). This requires a single matrix inversion in every iteration step. For computational efficiency, this is accomplished using multigrid iteration (cf [8]).

3.3. Relaxing the assumption of a vanishing divergence

Due to out-of-plane motion (that can hardly be totally avoided), the assumption of a vanishing divergence will usually not hold in practice.

Let us therefore relax the assumption and minimize

$$\begin{aligned} &E = \frac{1}{2} \int_\Omega \{(u \cdot \nabla I + I_t)^2 + \lambda(\omega - \omega_T)^2 + \kappa|\nabla\omega|^2 + \mu|\mathrm{d}|^2\} \,\mathrm{d}x, \\ &\text{s.t.} \quad \nabla \cdot u = \mathrm{d}, \qquad \nabla \times u = \omega, \end{aligned} \tag{20}$$

where the 2D divergence d (which is assumed to be small) actually corresponds to the derivative of the out-of-plane component of u in the out-of-plane direction (i.e., $d = \partial u_3 / \partial x_3$). Note that we do not change the vorticity transport equation itself—we still assume that the 2D vorticity transport equation is able to give a good approximation for the transport process. Therefore, (20) should only be used to analyse 2D projections of incompressible fluids.

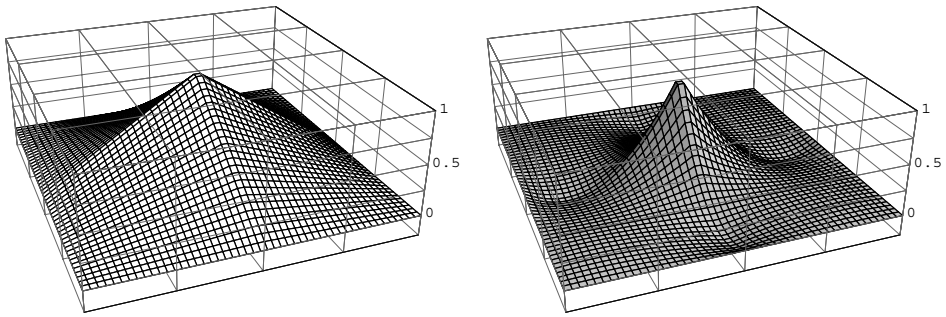

Figure 2. Left: basis function ϕ of a bilinear finite element. Right: basis function ψ of a biquadratic finite element.

4. Experimental evaluation

This experimental section is divided into three parts:

- Section 4.1 shows numerical results on ground truth fluid image sequences (2D flows) obtained with our approach in comparison with cross-correlation and optical flow with first-order and with higher order regularization.
- Section 4.2 shows numerical results for a synthetic flow where the out-of-plane component is not negligible (3D flow). We perform the analysis with the method introduced in section 3.3.
- In section 4.3, we finally show results for a real-world 2D image sequence.

4.1. Synthetic 2D flows

This section shows numerical results on ground truth fluid image sequences obtained with our approach in comparison with cross-correlation and optical flow with first-order regularization and higher order regularization.

The synthetic PIV image sequence that we used for testing was provided by [4]. The underlying velocity field was computed by a so-called pseudo-spectral code that solves the vorticity transport equation in Fourier space and evaluates a subgrid model for simulating small-scale turbulent effects on the larger scales of the flow. These latter effects are *not* known in practice, of course, and consequently they were ignored while evaluating our approach.

In order to simulate the intensity function of real PIV images, the computed velocity fields are used to transport collections of (images of) particles that are typically used for the seeding of flows so as to make them visible (cf section 1.1). The scheme resembles the one described in [14]. We used the first 100 frames of the synthesized PIV image sequence and compared the following three approaches:

- *Multi-pass cross-correlation* [11]. Advanced cross-correlation approach (LaVision Davis 7.1.1.34). Initial interrogation window size 32×32, final interrogation window size 8×8 and 50% overlap manually selected for best performance. In order to interpolate the velocity vectors to the fine grid (i.e., one vector per pixel), second-order spline interpolation is used.
- *Horn and Schunck* [9]. First-order regularization, temporal coherency is not exploited, no incompressibility constraint is imposed. The smoothness parameter $\lambda = 0.005$ was manually selected for best performance.
- *Second-order regularization* [27]. These authors used higher order regularization with an additional incompressibility constraint. Instead of mixed finite elements (as we do), the authors used the so-called mimetic finite differencing scheme. Temporal coherency is not exploited. Parameters: $\lambda_1 = 0.5, \lambda_2 = 0.05$, manually selected for best performance.
- *Optical Stokes flow* [22]. Optical flow approach that incorporates physical prior knowledge. Admissible flow fields are restricted to vector fields satisfying the Stokes equation. Parameters: $\mu = 1, \alpha = 100, \beta = 100, \gamma = 200$ manually selected for best performance. Temporal coherency is not exploited.
- *Vorticity transport approach (this paper).* As described above, higher order regularization is used, the incompressibility constraint is imposed, and temporal coherency is exploited in an on-line manner. Parameters: $\lambda = 0.005, \mu = 0.005, \nu = 0.1, \kappa = 0.0005$. As for the other approaches, we selected the regularization parameters λ, μ, κ by hand. Note that the viscosity coefficient ν is not a free user parameter but characterizes the physical nature of the fluid flow. Choosing a different value may affect the accuracy of the predictor (3). Parameter λ is the only intrinsic user parameter of our approach that weights the influence of the prediction ω_T in (8), whereas μ and κ are merely constants to achieve numerical stability as explained in connection with (8) and (16).

Figure 4 compares the errors of all five approaches over time. The multi-pass cross-correlation approach's estimate has the highest RMS error. This is due to the very high velocity frequencies that are present in the image data and that cannot be recovered by correlation. First-order regularization yields a higher error than second-order regularization which is much more accurate. The quality of the estimation can further be improved by applying optical Stokes flow. The errors of all four of these approaches stay constant over time because each subsequent image pair is independently evaluated and temporal coherency is ignored.

For the first frame, the approach presented in this paper, utilizing the vorticity transport equation, shows worse performance than the other optical flow-based algorithms. During the subsequent period of time, however, the error of the vorticity transport approach decreases considerably, because not only is higher order regularization used but temporal coherency is successfully exploited as well.

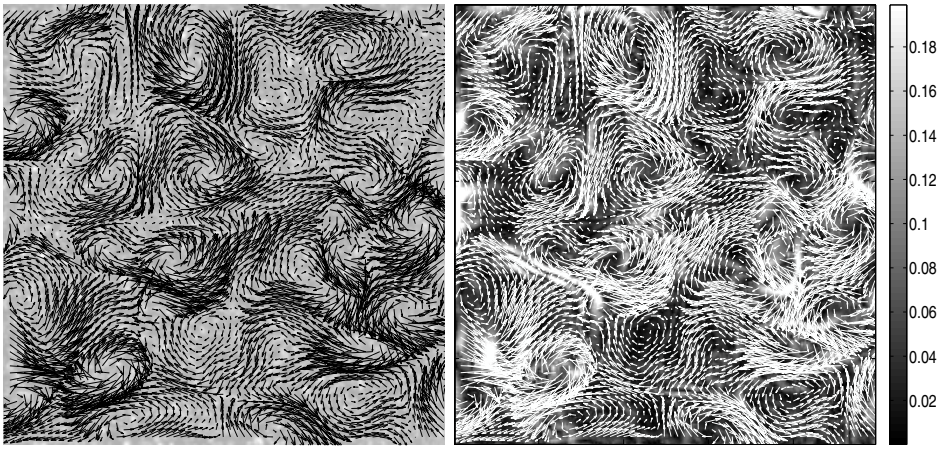

Figure 3. Left: 100th frame of the synthetic image sequence with ground truth velocity field. Right: estimated velocity field for the 100th frame. The background intensity shows the absolute RMS error (brighter = larger error), which is about 0.055 px. on average (cf figure 4).

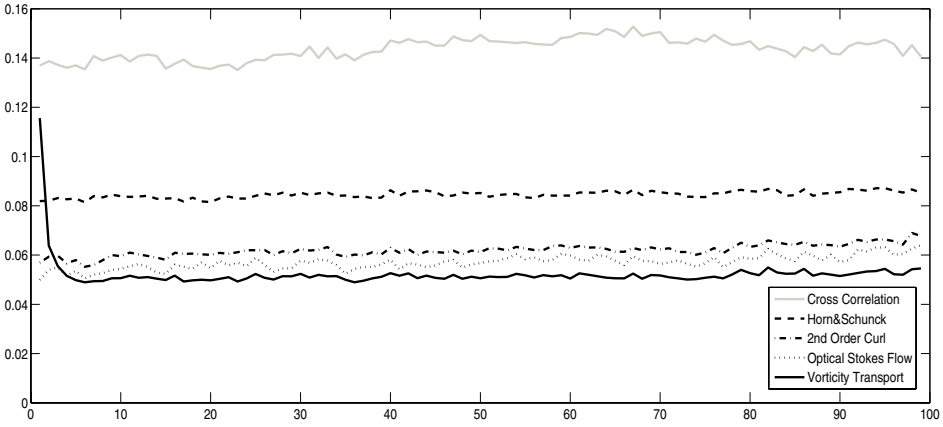

Figure 4. Average absolute RMS error (in pixels) for frames 1–100, using five different methods. Cross-correlation gives the worst results for this highly non-rigid image pair. First-order regularization performs worse than second-order regularization, while optical Stokes flow is slightly better than second-order regularization. All four of these error curves are constant because temporal coherency is not exploited. The approach based on vorticity transport starts with a rather low accuracy (assumption of $\omega = 0$, which is not valid) but then becomes significantly more accurate than the other techniques due to the physically consistent regularization over time. This novel spatio-temporal regularization is achieved with an on-line computational scheme and fixed storage requirements, irrespective of the length of the image sequence. The decay of the error curve within the first ten frames clearly displays the usage of this implicitly encoded 'memory'.

We emphasize that temporal coherency does *not* mean smoothness. Rather, the flow exhibits high spatio-temporal gradients as turbulent fluids do. Temporal coherency relates to a physically consistent transport mechanism interacting with flow estimation from an image sequence. Due to the on-line computational scheme, fixed computational resources are needed no matter how long the image sequence is. The decay of the error curve over several frames in figure 4 shows, however, that the approach is able to memorize the history longer than just the previous frame.

Figure 3 displays the estimated velocity for the 100th frame, along with the respective RMS errors. The reconstructed velocity field is surprisingly exact, in view of the highly non-rigid motion we are dealing with. Figure 5 shows that even the vorticity related to flow *derivatives* is reconstructed quite well under these difficult conditions. We expect such quantitative data to be valuable information in connection with imaging-based fluid mechanics.

4.2. Flows with out-of-plane velocity component

In order to assess our approach's performance when it comes to tackling image sequences with a high out-of-plane component, we analysed the VSJ image sequence 301 [15]: it shows a 3D jet shear flow with an out-of-plane component up to 4 pixels[3]. Due to the large out-of-plane velocity component, the assumption of vanishing divergence does not hold in this example. This is why we weaken the assumption of vanishing divergence as shown in section 3.3.

Figure 6 compares the results of our vorticity transport approach with those of an advanced cross-correlation approach (DaVis). For the evaluation, we chose the following parameters:

- *Multi-pass cross-correlation.* Initial interrogation window size 32 × 32, final interrogation window size

[3] Note that we assume that the imaginary grid in the out-of-plane direction has the same resolution as the in-plane grid.

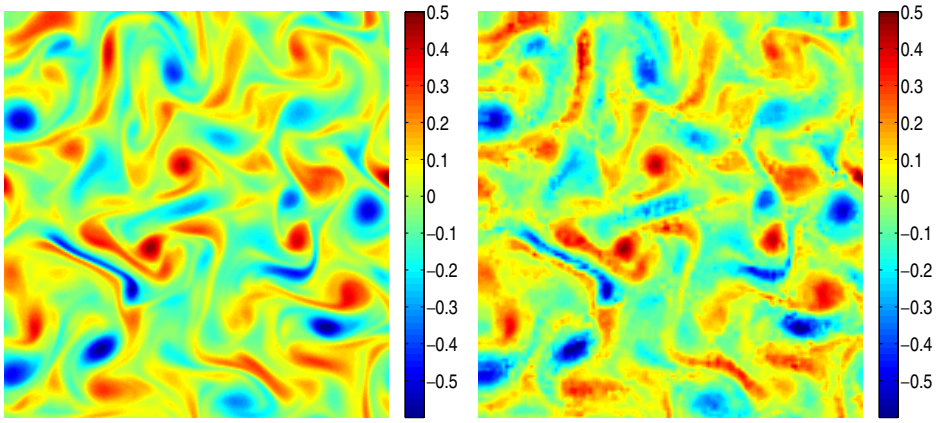

Figure 5. Left: true vorticity of frame 100. Right: estimated vorticity ω for frame 100. For the first frame, the estimation process was initialized with $\omega = 0$, corresponding to 'nothing is known in advance'. The result on the right shows that not only has the vorticity transport equation been successfully adapted to the observed image sequence, but that it improves the accuracy of flow estimation in terms of u, too (cf figure 4). As a consequence, flow *derivatives* can be estimated fairly accurate, as shown in the right panel. Such quantitative information is very important in connection with imaging-based experimental fluid mechanics.

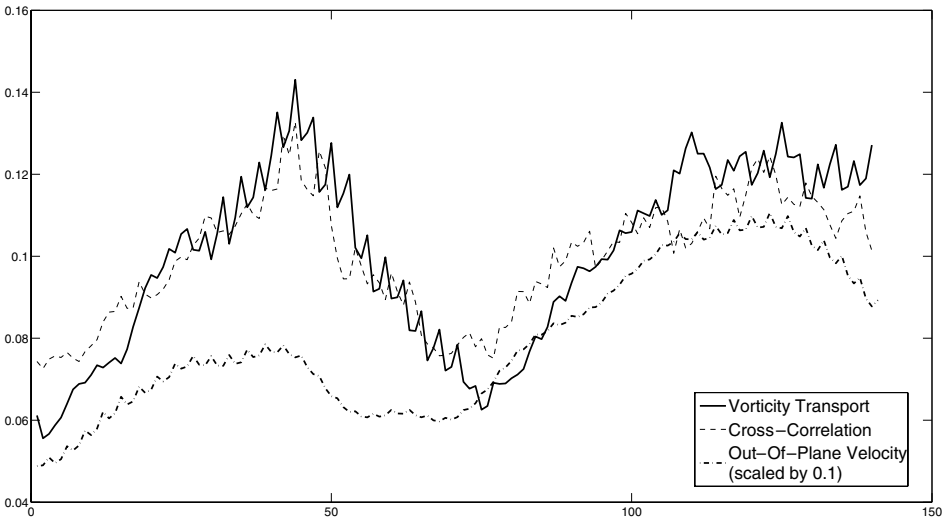

Figure 6. Average absolute RMS error (in pixels) for frames 1–140 of the VSJ 301 image sequence, using cross-correlation and novel optical flow technique with spatio-temporal regularization (with modification of section 3.3). Both approaches have similar accuracy.

16×16 and 50% overlap, manually selected for best performance.

- *Vorticity transport approach (this paper).* $\lambda = 0.005$, $\mu = 0.005$, $\nu = 0.1$, $\kappa = 0.005$, manually selected for best performance.

Figure 6 shows the absolute RMS error of both approaches along with the average absolute out-of-plane motion over time. While both error curves are quite similar, the cross-correlation approach tends to give better results at time instances when the out-of-plane velocity is rather large (i.e., $t \approx 40$ and $t \approx 125$) whereas the optical flow results are better when the out-of-plane component is rather small (i.e., $t \approx 1$ and $t \approx 70$).

The fact that the brightness of particles that travel out of the illuminated plane fades, while particles gain brightness if they travel towards the illuminated plane is in contradiction with the optical flow constraint that we use. This introduces errors in scenarios where high out-of-plane velocities are present. We would like to stress, however, that cross-correlation approaches have the same problem (as they also assume brightness conservation), it just seems to be slightly less pronounced. In section 5, we will briefly discuss possible improvements that might enhance the quality of optical flow based approaches in environments with high out-of-plane velocities.

4.3. Real-world 2D flows

Figure 7 shows a sample image of the experimental evaluation of the spreading of a low diffusivity dye in a 2D turbulent flow, forced at a large scale. The passive scalar is a mixture of fluorescein and water. For more details about the experimental setup, we refer to [12]. Cross-correlation approaches are not able to extract valid velocity fields for this type of input data (passive scalar images). Figure 7 shows, however, that our approach using the vorticity transport equation is capable of

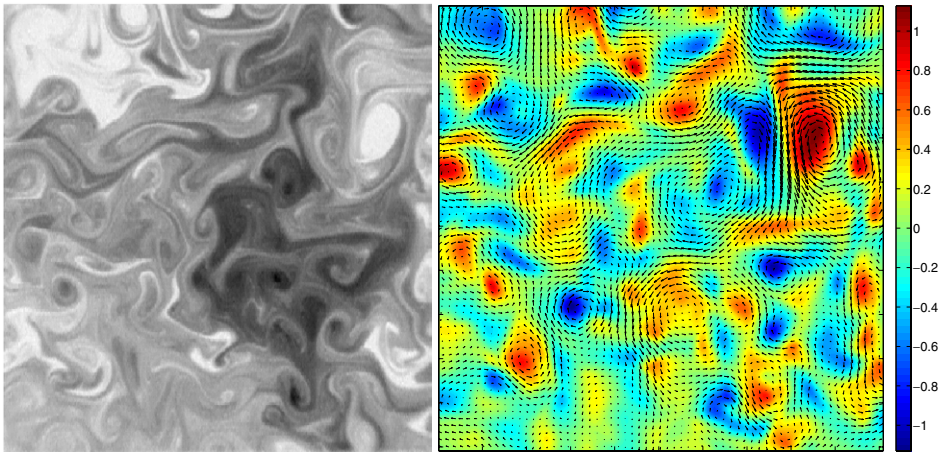

Figure 7. Left: sample real-world passive scalar image (frame 80, size: 512 × 512). Right: recovered velocity field (with colour-coded vorticity) with vorticity transport approach.

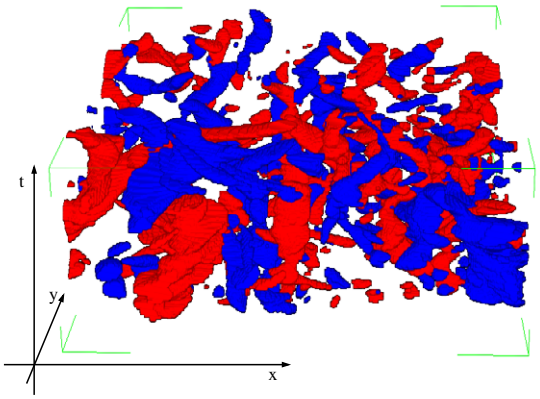

Figure 8. Iso-surface plot of the vorticity distribution over time. Blue denotes positive vorticity ($\omega > 0.75$) and red denotes negative vorticity ($\omega < -0.75$).

extracting a very reasonable velocity distribution. Figure 8 shows the temporal evolution of individual vortices.

5. Conclusions and further work

We presented an approach to fluid motion estimation that uses the vorticity transport equation for physically consistent spatio-temporal regularization. The approach combines variational motion estimation with higher order regularization and motion prediction through a transport process. For motions that conform to our assumption (i.e., fluids that are governed by the incompressible 2D Navier–Stokes equation), a temporal regularization effect, computed in a recursive manner, was demonstrated. In these scenarios, our approach outperforms cross-correlation approaches as well as advanced variational approaches for optical flow estimation.

In our future work we will focus on two major issues:

- *Adaptive optical flow constraint.* While we have adapted our regularization term to handle large out-of-plane motions, the optical flow constraint forming the data term in our current approach is only valid for 2D flows. In the future, we will replace the simple optical flow constraint by a more advanced data term that is able to deal with brightness variations that are caused by out-of-plane motion and illumination changes in 2D scenarios.
- *Three-dimensional flow analysis.* Imposing physical constraints is much more straightforward in 3D (no need to handle out-of-plane motion separately, cf section 3.3), but poses new computational challenges as well. As there is a lot of progress regarding capturing devices (e.g., scanning PIV or tomographic PIV), we will concentrate on full 3D flow analysis and related variational models and computational estimation schemes.

Acknowledgments

The authors thank Johan Carlier (Cemagref) for providing the 2D image sequences and Rainer Hain (TU Braunschweig) for providing the cross-correlation estimates. Support by the Deutsche Forschungsgemeinschaft (DFG, SCHN 457/6) within the priority programme ‘Bildgebende Messverfahren in der Strömungsmechanik’ (www.spp1147.tu-berlin.de) and by the EU-project ‘Fluid Image Analysis and Description’ (http://fluid.irisa.fr/) is gratefully acknowledged.

References

[1] Bertalmio M, Bertozzi A and Sapiro G 2001 Navier–Stokes, fluid dynamics, and image and video inpainting *Proc. IEEE CVPR* pp 355–62
[2] Braess D 1997 *Finite Elements. Theory, Fast Solver, and Applications in Solid Mechanics* (Berlin: Springer)
[3] Brezzi F and Fortin M 1991 *Mixed and Hybrid Finite Element Methods* (New York: Springer)
[4] Carlier J and Heitz D 2D turbulence sequence provided by Cemagref within the European Project ‘Fluid Image Analysis and Description’ (http://fluid.irisa.fr/)
[5] Corpetti Th, Heitz D, Arroyo G, Mémin E and Santa-Cruz A 2005 Fluid experimental flow estimation based on an optical-flow scheme *Exp. Fluids* **40** 80–97
[6] Fortin M and Glowinski R 1983 *Augmented Lagrangian Methods: Applications to the Numerical Solution of Boundary-Value Problems* (Amsterdam: North-Holland)
[7] Gunzburger M D 2002 *Perspectives in Flow Control and Optimization* (Philadelphia, PA: SIAM)

[8] Hackbusch W 1993 *Iterative Solution of Large Sparse Systems of Equations (American Mathematical Society* vol 95) (Berlin: Springer)
[9] Horn B and Schunck B 1981 Determining optical flow *Artif. Intell.* **17** 185–203
[10] Kohlberger T, Mémin E and Schnörr C 2003 Variational dense motion estimation using the Helmholtz decomposition *Scale Space Methods in Computer Vision (Lecture Notes in Computer Science* vol 2695) ed L D Griffin and M Lillholm (Berlin: Springer) pp 432–48
[11] LaVision 2005 *DaVis. Software for Intelligent Imaging*
[12] Jullien M C, Castiglione P and Tabeling P 2001 Intermittency of a passive tracer in the inverse energy cascade *Phys. Rev.* E **64** 035301
[13] Michaewicz Z 1994 *Genetic Algorithms + Data Structures = Evolution Programs* (Berlin: Springer)
[14] Okamoto K, Nishio S and Kobayashi T 2000 Standard images for particle-image velocimetry *Meas. Sci. Technol.* **11** 685–91
[15] Okamoto K, Nishio S, Kobayashi T, Saga T and Takehara K 2000 Evaluation of the 3D-PIV standard images (PIV-std project) *J. Vis.* **3** 115–24
[16] Okuno T, Sugii Y and Nishio S 2000 Image measurement of flow field using physics-based dynamic model *Meas. Sci. Technol.* **11** 667–76
[17] Paragios N, Chen Y and Faugeras O (ed) 2005 *The Handbook of Mathematical Models in Computer Vision* (Berlin: Springer)
[18] Puckett E G and Colella P 2005 *Finite Difference Methods for Computational Fluid Dynamics (Cambridge Texts in Applied Mathematics)* (Cambridge: Cambridge University Press)
[19] Raffel M, Willert C and Kompenhans J 2001 *Particle Image Velocimetry* (Berlin: Springer)
[20] Ruhnau P, Gütter C and Schnörr C 2005 A variational approach for particle tracking velocimetry *Meas. Sci. Technol.* **16** 1449–58
[21] Ruhnau P, Kohlberger T, Nobach H and Schnörr C 2005 Variational optical flow estimation for particle image velocimetry *Exp. Fluids* **38** 21–32
[22] Ruhnau P and Schnörr C 2007 Optical Stokes flow estimation: an imaging based control approach *Exp. Fluids* **42** 61–78
[23] Stahl A, Ruhnau P and Schnörr C 2006 A distributed-parameter approach to dynamic image motion *Int. Workshop on The Repres. and Use of Prior Knowl. in Vision, ECCV 2006 (Lecture Notes in Computer Science)* (Berlin: Springer) at press
[24] Suter D 1993 Mixed finite elements and Whitney forms in visual reconstruction *Proc. SPIE: Geometric Methods in Computer Vision II* **2031** 51–62
[25] Suter D 1994 Mixed-finite element based motion estimation *Innov. Tech. Biol. Med.* **15** 292–307
[26] Weickert J and Schnörr C 2001 Variational optic flow computation with a spatio-temporal smoothness constraint *J. Math. Imaging Vision* **14** 245–55
[27] Yuan J, Ruhnau P, Mémin E and Schnörr C 2005 Discrete orthogonal decomposition and variational fluid flow estimation *Scale-Space 2005 (Lecture Notes in Computer Science* vol 3459*)* (Berlin: Springer) pp 267–78